An Electromechanical Model of the Myocardium for Cardiac Image Analysis and Medical Simulation

Maxime Sermesant, Hervé Delingette, Nicholas Ayache

INRIA

INSTITUT NATIONAL DE RECHERCHE EN INFORMATIQUE ET EN AUTOMATIQUE

An Electromechanical Model of the Myocardium for Cardiac Image Analysis and Medical Simulation

Maxime Sermesant — Hervé Delingette — Nicholas Ayache

N° 5395

26 Novembre 2004

Thème BIO

ISSN 0249-6399 ISRN INRIA/RR--5395--FR+ENG

INRIA
SOPHIA ANTIPOLIS

An Electromechanical Model of the Myocardium for Cardiac Image Analysis and Medical Simulation

Maxime Sermesant*† , Hervé Delingette † , Nicholas Ayache †

Thème BIO — Systèmes biologiques
Projet Epidaure

Rapport de recherche n° 5395 — 26 Novembre 2004 — 25 pages

Abstract: This research report presents a new 3D electromechanical model of the two cardiac ventricles designed both for the simulation of their electrical and mechanical activity, and for the quantitative analysis of time series of medical images. First, we present a method to build volumetric biomechanical models based on different information sources. Then the action potential propagation is simulated using FitzHugh-Nagumo reaction-diffusion equations. The myocardium contraction is modelled through a rheologic law including an electromechanical coupling. Simulation of a cardiac cycle, with boundary conditions representing blood pressure and volume constraints, leads to the correct estimation of global and local parameters of the cardiac function. This model enables the introduction of pathologies and the simulation of electrophysiology interventions. Then a new pro-active deformable model of the heart is introduced to track the two ventricles in time series of cardiac images. Preliminary results indicate that this pro-active model, which integrates a priori knowledge on the cardiac anatomy and on its dynamical behaviour, can improve the accuracy and robustness of the extraction of functional parameters from cardiac images even in the presence of noisy or sparse data. Such a model also allows the simulation of cardiovascular pathologies in order to test therapy strategies and to plan interventions.

Key-words: Cardiac Modelling, Cardiac Image Analysis, Deformable Model, Electromechanical Coupling, Simulation of Cardiac Pathologies

* corresponding author: maxime.sermesant@centraliens.net. Maxime Sermesant is now with the Cardiac MR Research Group, King's College London, Guy's Hospital.
† Epidaure Research Project, INRIA Sophia Antipolis, 2004 Route des Lucioles, BP 93, 06 902 Sophia Antipolis, France

Unité de recherche INRIA Sophia Antipolis
2004, route des Lucioles, BP 93, 06902 Sophia Antipolis Cedex (France)
Téléphone : +33 4 92 38 77 77 —Télécopie : +33 4 92 38 77 65

Modèle électromécanique du myocarde pour l'analyse d'images cardiaques et la simulation médicale

Résumé : Ce rapport présente un modèle dynamique de l'activité électromécanique du cœur pour l'analyse de séquences temporelles d'images et la simulation médicale. Tout d'abord, un processus de construction de modèles biomécaniques volumiques du myocarde à l'aide de maillages tétraédriques est mis en place. Puis la propagation du potentiel d'action dans le myocarde est simulée, en se fondant sur des équations aux dérivées partielles de réaction-diffusion de type FitzHugh-Nagumo, qui permettent l'inclusion de pathologies et la simulation d'interventions. Ensuite, la contraction du myocarde est modélisée sur un cycle cardiaque grâce à une loi de comportement incluant un couplage électromécanique et des conditions limites intégrant l'interaction avec le sang. Ce modèle est ainsi validé à travers certains paramètres globaux et locaux de la fonction ventriculaire cardiaque. Une fois ce modèle électromécanique mis en place, il est utilisé dans une méthode de segmentation par modèle déformable de séquences d'images médicales, afin d'en extraire des paramètres quantitatifs de la fonction cardiaque. Cette nouvelle génération de modèles déformables pro-actifs permet d'intégrer de l'information a priori non seulement sur l'anatomie et le comportement mécanique mais aussi sur l'activité électrique et le mouvement. Le couplage au sein d'un même modèle d'informations anatomiques, biomécaniques et physiologiques contribue à améliorer la robustesse et la précision face à des données bruitées et éparses comme les images médicales et ouvre des possibilités supplémentaires en simulation médicale.

Mots-clés : modélisation cardiaque, analyse d'images cardiaques, modèles déformables, couplage éléctromécanique, simulation de pathologies cardiaques

1 Introduction

In this research report, we introduce a new integrated 3D model of the left and right ventricles of the heart which can be used for the simulation and the analysis of cardiac pathologies. The overall principle is described in Figure 1, where our *in silico* model includes knowledge coming from various disciplines including anatomy, electrophysiology and biomechanics. The parameters of this model can then be compared to clinical data in order to adjust the model to the observations. The adjusted model can reveal a number of parameters useful for the analysis of the cardiac function. It can also be used to simulate a number of pathologies (e.g. local ischemia) or the effect of therapeutic actions (e.g. radio-frequency ablation), by varying a number of local parameters for instance conductivity or contractility.

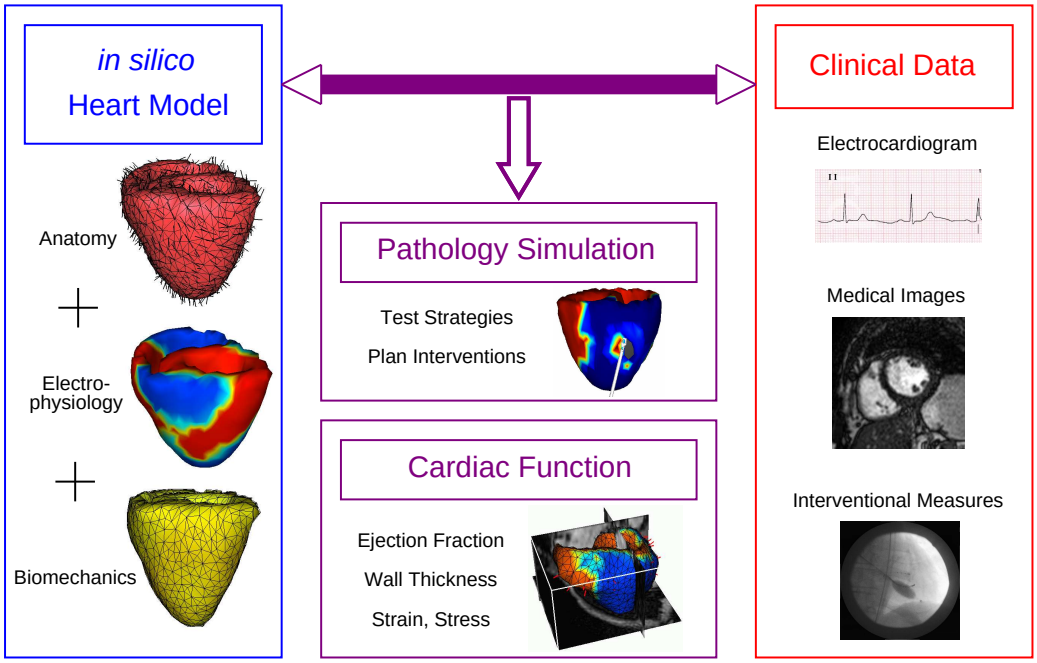

Figure 1: Overview: electromechanical model of the heart construction, interaction with patient data and applications: simulation of cardiac activity for pathology simulation and clinical data analysis.

Modelling of the human body has been of increasing interest in the last decades [4], as progresses in biology, physics and computer science made it conceivable. It is now possible to combine *in vivo* observation, *in vitro* experiments and *in silico* simulations.

There is a huge literature on the functional imaging and modelling of the heart [30, 42]. The following references provide examples of the measurement of electrical activity, deformation, flows, fibre orientation [41, 12, 43, 32, 60], and of the modelling of the electrical and mechanical activity of the heart [44, 26, 53]. Many of the functional models of the heart are direct computational models, designed to reproduce in a realistic manner the cardiac activity, often requiring high computational costs and the manual tuning of a very large number of parameters. In our approach, we should rather select a level of modelling compatible with reasonable computing times and involving a limited number of parameters, thus allowing the potential future identification of the model parameters from clinical measurements on any specific patient (by solving the corresponding inverse problem). First work in this direction was presented in a symposium meeting [64].

Also we would like our model to help the interpretation of cardiac image sequences. Cardiac image segmentation is still an active research area as reported in the survey by Frangi *et al.* [15] and the special issue of IEEE TMI [16]. In the deformable model framework [45], mainly deformable surfaces have been used in segmentation methods [48]. A combination of spatial and time constraints in such models was proposed in [47]. Whereas it ensures a better robustness against noise and can include trajectory constraints, there is no *a priori* knowledge introduced on the motion to help the segmentation. To go further, a three-dimensional deformable surface is combined with a four-dimensional statistical heart motion model computed from series of tagged MR images in [17]. This motion model allows a better initialisation in the different images from a segmentation of the first image, thus a better segmentation of the sequence. Another extended approach presented in [31] combines a Point Distribution Model (PDM) and two coupled triangulated surfaces to segment the left ventricle, using also

a motion model for the initialisation. Deformable surfaces can also be coupled with prior segmentation, for instance multi-scale fuzzy-clustering [63].

Extensions of the PDMs used in segmentation methods are based on the Active Shape Models (ASM) and the Active Appearance Models (AAM). A description and comparison of these two models can be found in [10]. These models are now developed for spatio-temporal data. In [21], the ASM is extended to 2D+time by introducing spatio-temporal shapes (ST-shapes). In [35], the AAM framework is extended to 2D+time by considering the image sequence as a single shape/intensity sample, giving the Active Appearance Motion Model (AAMM). These models can be theoretically extended to 3D, but the size of the models and the difficulty to obtain good correspondences in 3D images make it still a current research area.

At the same time, deformable templates evolved toward sophisticated approaches, for instance combined with Bayesian classification and Markov random fields [46], or coupling shape-space and Kalman-filter-based tracking [28]. But few of these approaches integrate the volumetric aspect of human organs and the dynamic nature of the heart. Due to the complexity of the developed methods, it is mostly done by propagating the result obtained in one image (or one slice) to the next one [29].

Volumetric models have mostly been introduced in cardiac function analysis for interpretation [56, 57], as they offer richer mechanical parameters. They were also introduced in deformation analysis for physically-based interpolation [13, 71, 5]. We believe that volumetric models also allow one to introduce much more *a priori* knowledge on the organ directly in the segmentation process. It can be anatomical information, like fibre orientation, or mechanical behaviour, to offer more reliable estimations of heart kinematics [55, 58, 70, 66, 38]. It can also be used to jointly estimate kinematics and mechanical properties of the myocardium [37]. Most of these approaches use hexahedral or tetrahedral meshes, but there are also alternative mesh-free methods proposed [36].

These models (geometrical and/or biomechanical) are passive models, i.e. they do not anticipate the cardiac motion, they only evolve under the action of 1) external image forces and 2) internal forces which constrain the regularity of the motion (geometrical models) or take into account the fibre orientations and a constitutive law (biomechanical models).

The key idea in this report is to build a "Pro-Active Deformable Model" of the heart for image analysis. It is a volumetric deformable model of the heart integrating *a priori* knowledge on the motion in the segmentation process through the simulation of the electrical propagation and the mechanical contraction. In the classification proposed by Frangi *et al.* review [15], the presented method would fit in the "continuous volumetric model" class. We believe that this new generation of physiology-based deformable models opens new possibilities in cardiac function analysis.

The pro-active model we introduce here presents an internal energy which creates a complete contraction of the two ventricles synchronised with the ECG, therefore the external forces only have to create local corrections to adjust the model to the boundaries observed in the cardiac images.

Using a model with physics- and physiology-based parameters makes it also possible to simulate some cardio-vascular pathologies and interventions. For instance, this could help devise techniques to make electrophysiology studies to correct abnormal heart rhythms shorter, less invasive and more successful.

The electromechanical model of the heart presented is based on mathematical systems of non-linear partial differential equations, set on a three dimensional domain, considering the ventricles as a continuum.

We present first the anatomical mesh construction, then the electrophysiology modelling and the contraction simulation, through an electromechanical coupling. This is validated against measures from both the literature and medical images. Finally two applications are presented: pathology simulation and segmentation of a cardiac image sequence.

2 Anatomical Model Construction

The myocardium is represented as a tetrahedral volumetric mesh including anatomical information. The process to build such a model is detailed in [66]. The main anatomical information we use is the myocardium geometry, its division into different anatomical parts and the local orientation of the muscle fibres.

2.1 Volumetric Mesh Creation

The geometry can be extracted from different medical imaging modalities. From a 3D image of the heart, the myocardium is segmented, using classical image processing methods like thresholding and mathematical morphology. Then, a triangulated surface of the myocardium is obtained using the marching cubes method [39],

and is decimated to the required size (typically 5000 nodes for accurate simulation, or 1000 nodes for the segmentation of cardiac images). Finally, a volumetric tetrahedral mesh is created from the triangulated shell, using the INRIA software GHS3D[1] (Fig. 2).

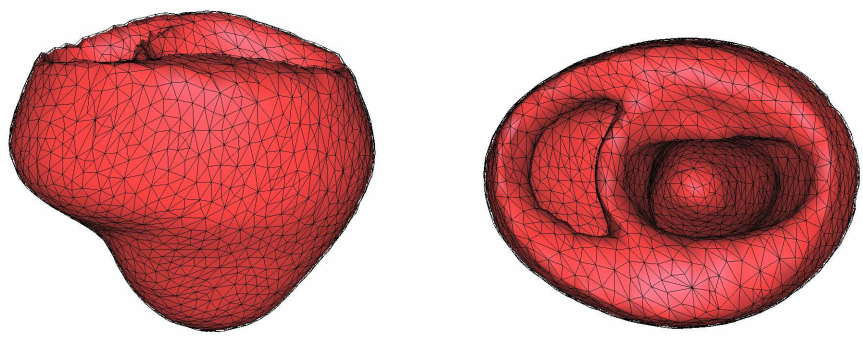

Figure 2: Tetrahedral mesh of the bi-ventricular myocardium (40 000 elements).

2.2 Anatomical Labelling

To better control and analyse the model during the simulation, we label the anatomical mesh into different regions. These regions were segmented in the myocardium from the Visible Human Project by Pr. Karl-Heinz Höhne group, Hamburg University [59]. This labelling is done by registering the mesh with the atlas image, and then assigning to each tetrahedron the class corresponding to the voxels whose centres are inside this tetrahedron (these voxels are obtained by rasterization, the whole procedure is detailed in [66]).

Fig. 3 presents the result of the anatomical regions attribution from the atlas to the mesh.

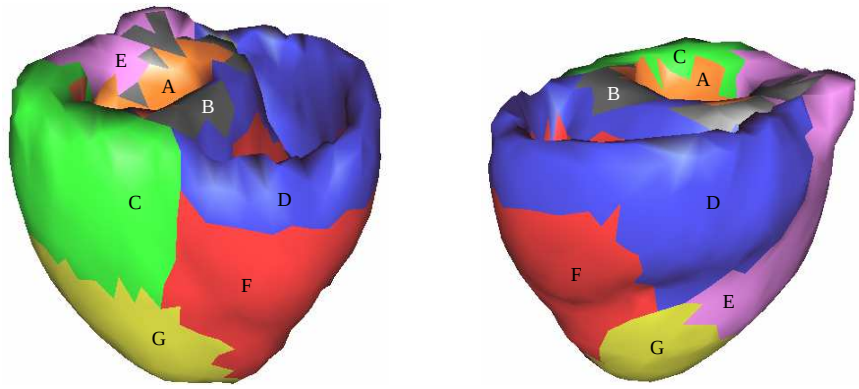

Figure 3: Anatomical regions obtained from the Visible Human atlas: Basal Left Endocardial Ventricle (A), Basal Septum (B), Dorsobasal Left Epicardial Ventricle (C), Basal Right Ventricle (D), Basal Left Epicardial Ventricle (E), Apical Right Ventricle (F), Apical Left Epicardial Ventricle (G).

2.3 Myocardial Fibre Orientations

The muscle fibre orientations can be obtained from dissection measures or diffusion tensor MR images (DTI) [23]. We present in this report the model built from the dissection measures performed on a canine heart in the bioengineering laboratory of the Auckland University, New Zealand[2]. This dataset was interpolated and smoothed by the bioengineering laboratory of the University of California, San Diego[3] [52].

The knowledge of the myocardial fibre orientations (Fig. 4) plays an important role in the realistic modelling of the electrical and mechanical activity of the heart. Indeed, the conductivity is typically four times larger

[1] http://www-rocq.inria.fr/gamma/ghs3d/ghs.html
[2] http://www.bioeng.auckland.ac.nz/home/home.php
[3] http://cmrg.ucsd.edu/

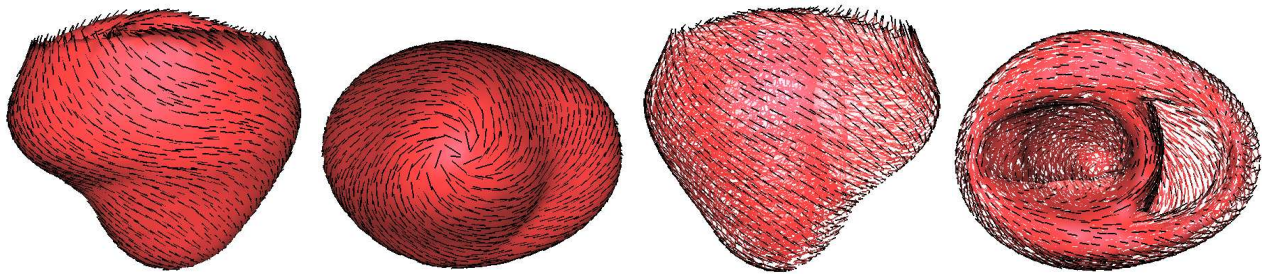

Figure 4: Fibre orientations assigned to the myocardium mesh from the data interpolated in UCSD.

along the fibres than in the transverse direction, the orientation of the fibres creates a strong anisotropy in the constitutive law of the material, and also constrains the direction of the contraction stress.

3 Electrophysiology: Action Potential Simulation

Many different models have been proposed to simulate the cardiac electrophysiology. They are divided in two main approaches:

- *biophysical* or *ionic* models: cellular level simulation, using as variables the concentrations of the different types of ions, and integrating different ion channels based on Hodgkin-Huxley equations [22, 6, 40, 54].
- *phenomenological* models: more macroscopic models using a simpler system of equations to compute the cell potential without explicitly computing the ions concentrations. It can be a bi-domain model, where the variables are the extra-cellular and intra-cellular potentials, or a mono-domain model where the variable is their difference, the action potential. It is based on FitzHugh-Nagumo system [14, 1, 33].

As we model the electrophysiology mostly to control the contraction, we use the second approach, because the contraction is mainly related to the action potential. Moreover, for clinical use, only the extra-cellular potential can be measured, not the different ions concentrations, so we could not adjust the parameters of the ionic approach from clinical data.

3.1 Action Potential

The action potential wave propagation is simulated using a system based on FitzHugh-Nagumo equations. This approach yields fast 3D computations and allows to capture the principal biological phenomena:

- a cell is activated only for a stimulus larger than a certain threshold;
- the shape of the action potential does not depend on the stimulus;
- there is a refractory period during which the cell cannot be excited;
- any cell can act as a pacemaker.

Aliev and Panfilov developed a modified version of the FitzHugh-Nagumo equations adapted to the dynamics of the cardiac electrical potential [1]:

$$\begin{cases} \partial_t u = \text{div}\,(D\,\nabla u) + ku(1-u)(u-a) - uz \\ \partial_t z = -(\varepsilon + \frac{\mu_1 z}{u+\mu_2})(ku(u-a-1)+z)) \end{cases} \tag{1}$$

u is a normalised action potential and z is a secondary variable for the repolarisation. k and ε control the repolarisation, and a the reaction phenomenon. This model is simplified here: the $\frac{\mu_1 z}{u+\mu_2}$ term represents the influence of pacing frequency on the action potential duration and this property is not needed at the moment, so this term is neglected. Parameter values are derived from [1]: $\varepsilon = 0.01$, $k = 8$, $a = 0.15$.

The orientation of the fibres is described by the 3×3 diffusion tensor D:

$$D = d_0 \begin{pmatrix} 1 & 0 & 0 \\ 0 & r & 0 \\ 0 & 0 & r \end{pmatrix}$$

in an orthonormal basis whose first vector is in the local fibre orientation. As previously mentioned, the conductivity in the fibre direction is typically four times larger than the conductivity in the transverse plane, therefore a typical value of r is $r = 0.25$. This yields a velocity of the propagation of the action potential typically two times faster in the fibre orientation than in the transverse plane (as the propagation speed of the action potential is proportional to the square root of the conductivity).

With an initial excitation above the threshold, the simulated action potential with this system is qualitatively similar to the action potential measured on cardiac cells (Fig. 5).

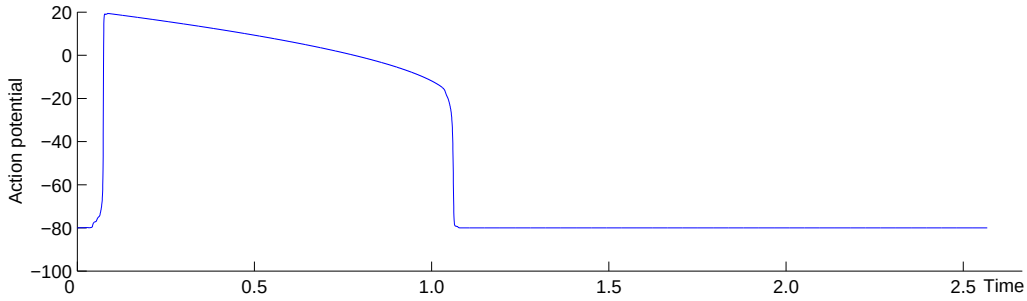

Figure 5: Simulation of action potential with simplified Aliev and Panfilov model. Time is normalised to obtain an action potential duration equal to 1 time unit.

3.2 3D Simulation of the Propagation

These equations are integrated on the 3D volumetric mesh defined in section 2. The dynamic propagation can be represented by displaying an isosurface of the action potential value. The complete propagation can be shown with the isochrones, where colours represent the different depolarisation times (Fig. 6).

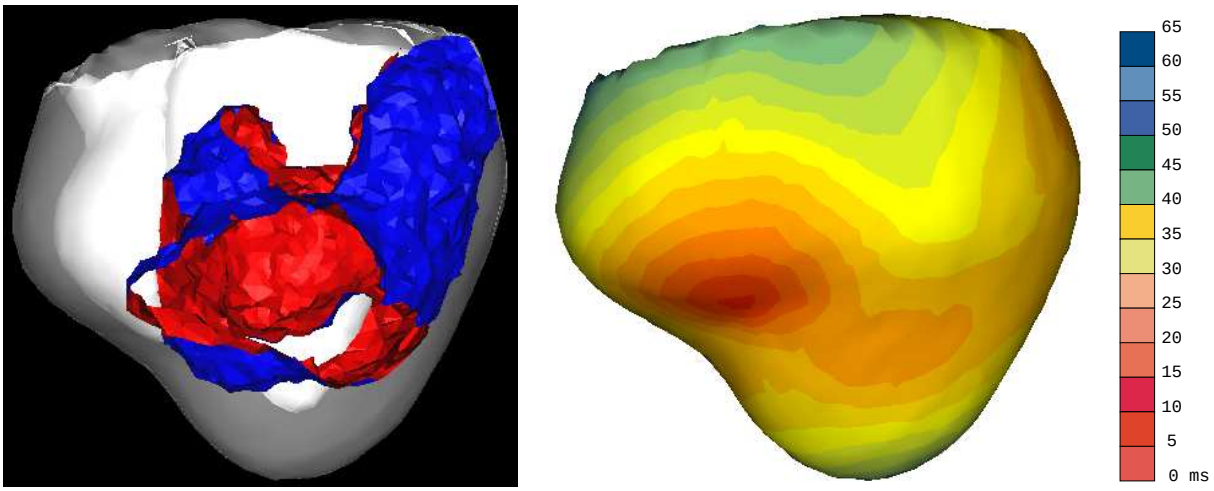

Figure 6: (Left) Isosurface of the simulated action potential value, representing the propagation front, at one instant of the cardiac cycle. (Right) Resulting isochrones after complete myocardium depolarisation.

3.3 Numerical Integration

The temporal integration is done with a fourth order Runge-Kutta scheme and the spatial integration is done with the Finite Element Method, using linear tetrahedral elements. The computation time step is 10^{-4} and a 3D simulation of the action potential during the cardiac cycle (0.85 s) takes around 5 mn on a standard PC with a 40 000 elements tetrahedral mesh.

4 Biomechanics: Electromechanical Constitutive Law and Boundary Conditions

4.1 Complex Mechanical Model

The myocardium is an active non-linear anisotropic visco-elastic material. Its constitutive law is complex and must include an active element for contraction, controlled by the action potential computed in the previous section, and a passive element representing the mechanical elasticity. Several constitutive laws have been proposed in the literature [27, 24, 19, 25, 51, 20, 8]. The one presented in this report is designed for clinical applications, in order to enable validation against clinical *in vivo* measures. It is based on the Bestel-Clément-Sorine model [7], which integrates in the Hill-Maxwell framework:

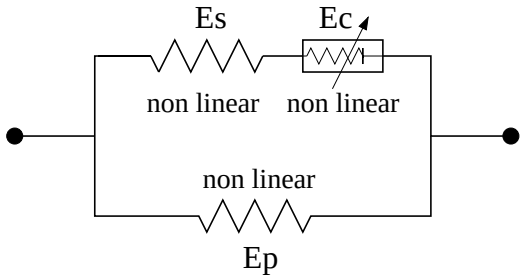

Figure 7: Hill-Maxwell framework used for Bestel-Clément-Sorine constitutive law.

and writes:

$$\begin{cases} \rho\ddot{P} - \mathrm{div}(K_p\,\mathcal{E}_p + C_p\,\dot{\mathcal{E}}_p + \sigma_c + C_c\,\dot{\mathcal{E}}_c + K_c\xi_0) = 0 \\ \partial_t K_c = K_0|u|_+ - (|\dot{\mathcal{E}}_c| + |u|)K_c \\ \partial_t \sigma_c = \sigma_0|u|_+ - (|\dot{\mathcal{E}}_c| + |u|)\sigma_c + K_c\dot{\mathcal{E}}_c \\ \sigma_c + C_c\,\dot{\mathcal{E}}_c + K_c\xi_0 = K_s(\mathcal{E}_p - \mathcal{E}_c) \end{cases} \tag{2}$$

with P the position, K the stiffness, C the damping, $\mathcal{E}$ the strain, σ the stress, u the normalised action potential and subscript c referring to the contractile element E_c, subscript p to the parallel element E_p and subscript s to the series element E_s. A detailed study of this complete model along with 1-dimensional simulations can be found in [9].

4.2 Simplified Mechanical Model

The electromechanical model proposed here is specifically designed for cardiac image analysis and simulation. It is built in order to be computationally efficient, so we chose to simplify the constitutive law of equation 2. The idea is to correct the simplification errors by using the available clinical information. In this framework, the model can be directly compared with *in vivo* measures through medical images, thus making a validation possible. Despite its simplicity compared to other constitutive laws proposed in the literature, it reproduces quite well the global and local behaviour of the myocardium.

The simplified mechanical model has the following components:

- a contractile element which creates a stress tensor σ_c, controlled by the action potential u;
- a parallel element which is anisotropic linear visco-elastic and creates a stress tensor σ_p.

For the electromechanical coupling, different laws have also been proposed [27, 51]. We chose a simple ordinary differential equation to control the coupling, directly computing the contraction intensity from the action potential. We believe that it is important to keep the model simple as not many clinical measures are available to adjust this law. The contractile element is controlled by the electrical action potential through the ODE:

$$\partial_t \sigma_c = \sigma_0|u|_+ - |u|\sigma_c$$

where $|u|_+$ is the positive value of u: $|u|_+ = u$ if $u > 0$, otherwise $|u|_+ = 0$.

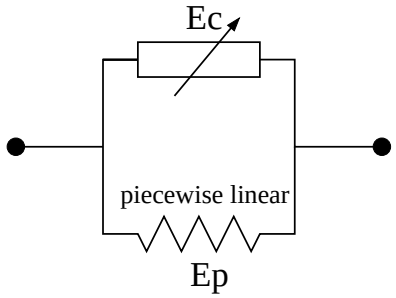

Figure 8: Scheme of the simplified rheological model.

As our action potential is normalised between 0 and 1, we can analytically approximate the solution of this equation with the following coupling model:

$$\sigma_c(t) = \begin{cases} \sigma_0 \left(1 - e^{\alpha_c (T_d - t)}\right) & \text{during depolarisation:} \quad T_d < t < T_r \\ \sigma_r e^{\alpha_r (T_r - t)} & \text{during repolarisation:} \quad T_r < t < T_d + HeartPeriod \end{cases} \tag{3}$$

with T_d the depolarisation time, T_r the repolarisation time, α_c the contraction rate, α_r the relaxation rate, and $\sigma_r = \sigma_c(T_r)$. We can add a constant to T_d and T_r in Eq. (3) to model the time delay between the electrical depolarisation and the mechanical contraction.

The tridimensional contraction stress tensor is obtained with the formula $\sigma_c f \otimes f$, where f denotes the fibre orientation and $\otimes$ the tensor product (for a column vector v, $v \otimes v = v.v^T$). In the dynamics equation, when integrated over an element, it results in the force vector:

$$F_c = \int_V \mathrm{div}(\sigma_c f \otimes f)\, dV = \int_S (\sigma_c f \otimes f)\, n\, dS$$

from Green-Ostrogradski formula, with n the surface normal, V and S the element volume and surface, respectively. Contraction force is thus equivalent to a pressure applied along the fibre orientation.

This simplified constitutive law is represented by a damping matrix C for the internal viscosity part, a stiffness matrix K for the transverse anisotropic elastic part (parallel element) and a force vector F_c computed from contraction (contractile element).

Once integrated into the dynamics equation, it writes:

$$M\frac{d^2U}{dt^2} + C\frac{dU}{dt} + KU = F + F_c \tag{4}$$

with U the displacement vector, M the diagonal mass matrix (mass lumping), C the Rayleigh damping matrix, K the anisotropic linear elastic stiffness matrix, F the different external loads from the boundary conditions and F_c the force vector from the contraction.

The behaviour of such a constitutive law is shown on a cubic volume in Figure 9. We can observe that the Lamé constants chosen to partly represent the incompressibility make the cube dilate vertically when it compresses horizontally.

4.3 Boundary Conditions: the Cardiac Phases

To simulate an entire cardiac cycle, the interaction of the myocardium with the blood is very important. This is why the different phases of the cardiac cycle have to be introduced, which implies different boundary conditions. The heart cycle can be divided in four phases: filling, isovolumetric contraction, ejection, and isovolumetric relaxation.

Four different boundary conditions are used on the mechanical model:

- *Filling*: a pressure is applied to the vertices of the endocardium. Its intensity is equal to the mean pressure of the atrium. It can be augmented during the P wave to introduce atrial contraction;
- *Isovolumetric contraction*: a penalty constraint is applied to the vertices of the endocardium to keep the ventricle volume constant;

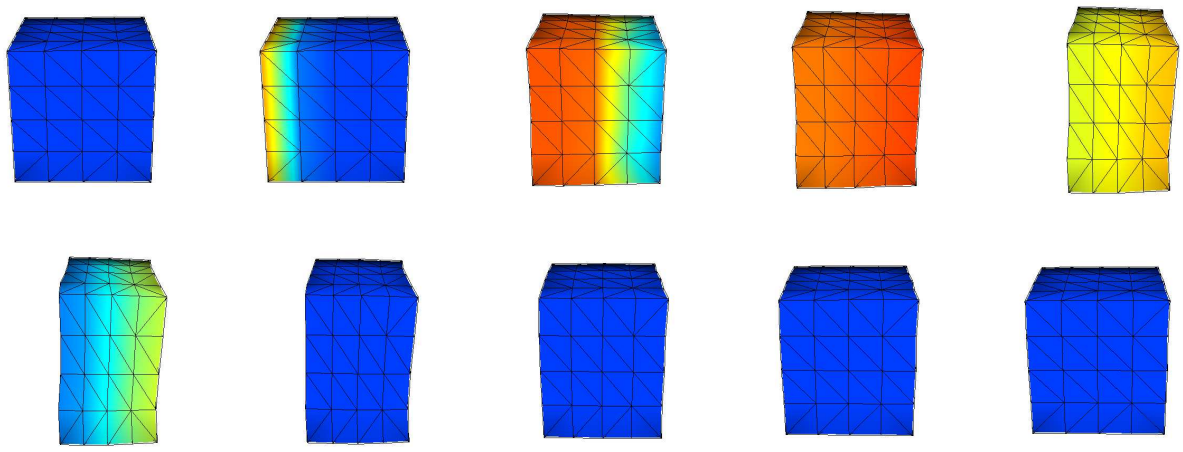

Figure 9: Contraction (first row) and relaxation (second row) simulation on a cube. Fibres are horizontal and an initial action potential is applied to the left facet of the cube. Colour represents the action potential value (dark blue: polarised, light red: depolarised).

- *Ejection*: a pressure is applied to the vertices of the endocardium. Its intensity is equal to the mean pressure of the aorta (for the left ventricle) and the pulmonary artery (for the right ventricle). It could be modulated with a Windkessel model to introduce artery compliance and resistance;
- *Isovolumetric relaxation*: a penalty constraint is applied to the vertices of the endocardium, keeping the volume constant.

To hold the mesh in space, we simulate the fibrous structure around the valves with springs having one extremity attached to a basal node and the other extremity attached to a fixed point.

In a first version, the succession of the different phases was triggered by a synchronisation mechanism based on a standard ECG. But this leads to non-continuous mechanical constraints which can create instabilities, as no information about the mechanical state of the model is used to change from one phase to another.

In the current version, the phase change is automatically controlled in the following way:

- during filling, a pressure is applied to the endocardium. When the contraction starts, the contraction force will tend to eject blood, so when this force is more important than the applied pressure, the blood flow (simply estimated as the volume time derivative) changes sign. This is used to close the atrial-ventricular valves and start the isovolumetric contraction.
- during the isovolumetric contraction, the applied penalty constraint counterbalances the contraction force, so it is directly equivalent to the intra-ventricular pressure. When the intensity of this penalty constraint is more important than the arterial pressure, the ventricular-arterial valves open, and the ejection phase starts.
- during ejection, contraction force decreases after repolarisation, so when it is less important than arterial pressure, the flow changes sign and the ventricular-arterial valves close, starting the isovolumetric relaxation phase.
- during isovolumetric relaxation, the penalty constraint represents the pressure, so when it is less important than atrial pressure, the atrial-ventricular valves open, starting the filling phase.

Even with these completely independent conditions for the left and right parts of the heart, the two ventricles stay well synchronised, which shows that force development is coherent in the model. It makes it possible to adjust contractility parameters from the length of the different phases, and also from the atrial and arterial pressures.

It is interesting to notice that these phase transitions are computed independently from the chosen constitutive law, so the biomechanics model can evolve without having to redesign the boundary conditions evolution.

4.4 Numerical Integration

The model is integrated in time using the Houbolt semi-implicit scheme, and in space using the Finite Element Method with tetrahedral linear elements, details of these methods can be found in many classical books, see [73] for instance. For the implementation we used the PETSc[4] library for linear algebra operations, thus allowing distributed matrix storage, parallel preconditioning and parallel iterative solving.

To achieve this electromechanical simulation, we have to integrate two different phenomena: electrophysiology and biomechanics, and each of the models has a distinct time step. If we call dt_e the electrical time step, dt_m the mechanical time step, and t_e (resp. t_m) the current electrical (resp. mechanical) integrated time since the beginning of the simulation, at each instant t of the cardiac cycle we integrate the least advanced phenomenon:

- if $t_e < t_m$: we integrate the electrical phenomenon, and then $t_e = t_e + dt_e$, $t = t + dt_e$;
- if $t_m < t_e$: we integrate the mechanical phenomenon, and then $t_m = t_m + dt_m$, $t = t + dt_m$;

The stability constraints from the boundary conditions are quite different during the different phases. We use an adaptive time step, with a time step 10^2 times smaller during the isovolumetric phases.

The whole electromechanical cardiac cycle simulation with these boundary conditions takes less than 30 minutes on a standard PC (40 000 elements tetrahedral mesh). Half of the simulation time is devoted to the computation of the isovolumetric phases even if they represent only around 15% of the heart cycle, because they require a much smaller mechanical time step to achieve stability.

5 Validation: Comparison of the Simulated Heart Cycle with Measures

5.1 Validation of the Action Potential Propagation

To simulate a realistic 3D propagation of the action potential in the myocardium we need to determine the electrical onset for the initial conditions. The sinoatrial node is the natural pacemaker, located within the wall of the right atrium. It generates electrical impulses that are carried by special conducting tissue to the atrioventricular node. After reaching the atrioventricular node, located between the atria and ventricles, the electrical impulse goes down a conducting tissue (the bundle of His) that branches into pathways that supply the right and left ventricles. These paths are called the right bundle branch and left bundle branch respectively. The left bundle branch further divides into two sub branches (called fascicles). The extremities of these bundles are the Purkinje network, creating the junction between this special conducting system and the myocardium.

For our simulation, we need to locate these Purkinje network extremities, but it is hardly visible by dissection or by medical imaging. We used the measures from Durrer *et al.* [11] which present the isochrones in an isolated human heart, paced from the special conducting system. The first isochrones allow to locate the Purkinje network extremities on the endocardia of both left and right ventricles (the colour version of these measures presented in Fig. 10 is available on the Internet[5]).

A first validation of the 3D computation consists of comparing the resulting action potential isochrones with the measures from Durrer *et al.*. As we can see in Fig. 10, our simulation is qualitatively very close to the reported measures.

We also used invasive measures on canine hearts from the Laboratory of Cardiac Energetics, National Heart, Lung, and Blood Institute, National Institutes of Health (NIH) to validate this model, the simulations and measures can be found in [65], and again excellent qualitative correspondences were achieved.

5.2 Validation of the Myocardium Contraction

One shows in this section that our model can reproduce a realistic motion of the two ventricles from a reduced set of easily controlled parameters. With a manual adjustment of the parameters σ_0, α_c, and α_r (see Eq. 3) we reproduced the motion of the heart observed in time series of 3D tagged Magnetic Resonance Images (MRI) [2], presented for the apico-basal rotation (Fig. 14), and for the radial contraction (Fig. 16). We are also able to produce curves for the left ventricle (LV) volume qualitatively similar to the curves extracted from the segmentation of MRI (Fig. 12).

[4] http://www-unix.mcs.anl.gov/petsc/petsc-2/index.html
[5] http://butler.cc.tut.fi/~malmivuo/bem/bembook/

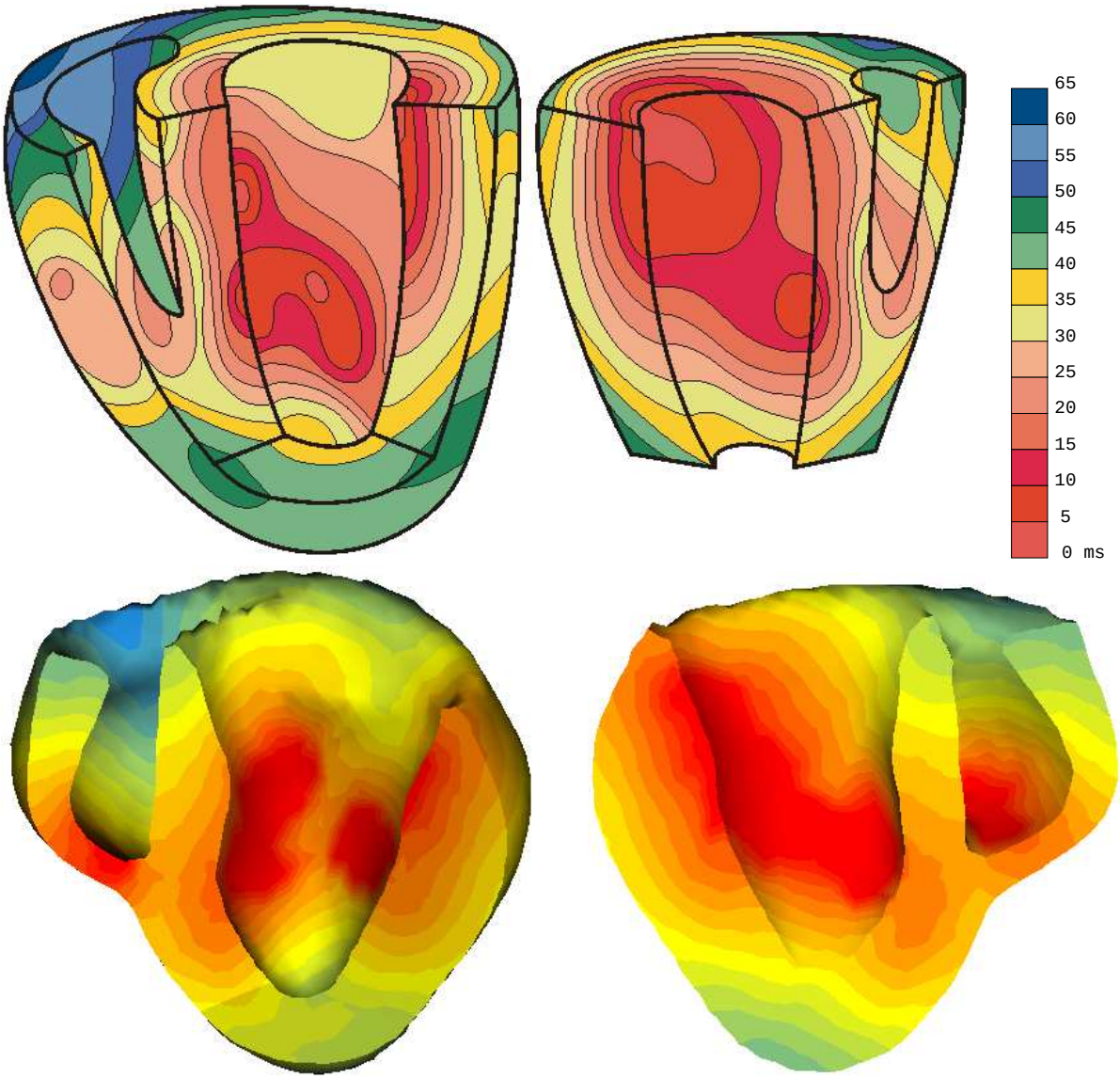

Figure 10: Action potential isochrones (in ms) measured by Durrer *et al.* (top row) compared with the simulated ones (bottom row).

The simulation results we present are plotted after two simulated cycles, in order to obtain "natural" initial conditions from periodicity.

5.2.1 Volume of the Ventricles

We define a set of triangles representing the endocardium of each ventricle and we then close this surface with the barycentre of its edge to compute the inner volume of the ventricles (red surfaces and green lines in Fig. 11).

The evolution of the ventricle volume during the simulation of the cardiac cycle (Fig. 12) is very similar to the data available in the literature (see [69] for instance). As we want to use this model for clinical applications, we also have to compare it with *in vivo* observations, i.e. medical imaging.

Automatic cardiac image segmentation is still a very challenging task, and manual segmentation of a full 4D sequence is long and tedious. We present here a comparison with a volume curve extracted from a 3D MRI sequence of a volunteer heart with the semi-automatic method detailed in [3].

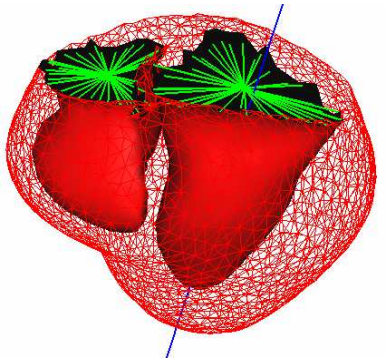

Figure 11: Triangles sets used to define the endocardia of each ventricle. The barycentres of the edges of these sets are used to close the ventricles in the volume computation.

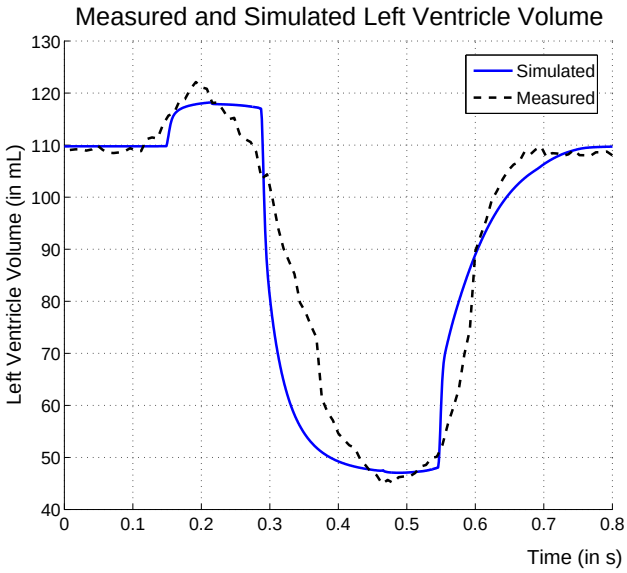

Figure 12: Measured left ventricle volume from MRI compared to the simulated cycle. The simulated volume values and the ejection fraction (60%) are similar to the ones measured in volunteer data (63%).

The simulated ventricle volume curve is qualitatively very similar to the measured one, with an ejection fraction of 60%, compared to 63% in the measures. The main differences are during phase transitions, which are times when the intra-ventricular volume definition is not trivial in the images.

We are currently introducing a Windkessel model, which is a classical model of the systemic compliance and resistance [62, 72], at the outflow of the ventricles. The arterial pressures would then increase during ejection, thus making the volume curve slope shallower. This is a more realistic model of the after-load, which is quite important in cardiac function, and should give results closer to the measures.

The evolution of these volumes makes it possible to adjust the contractility parameters (maximum contraction, contraction speed, relaxation speed) from the ejection fraction and the phase durations.

5.2.2 Local Apico-Basal Rotation

From the definition of the left ventricle endocardium, we can compute the inertia axis of the left ventricle (blue line in Fig. 11). We use this axis to compute the local apico-basal rotation of three points (Fig. 13) around this axis, throughout the cardiac cycle.

This same rotation was measured for different points of the myocardium by Philips Research France through the analysis of tagged MRIs [2].

The values from the simulation are very similar to the measures both qualitatively and quantitatively. Especially the opposite direction of rotation between the base and the apex is present both in the simulation

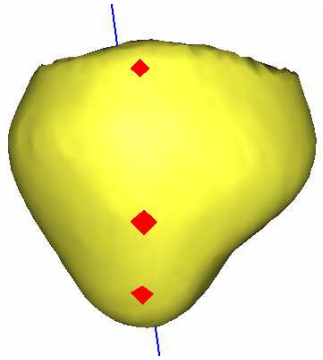

Figure 13: Basal, equatorial and apical points on the epicardium used to observe the local rotation during the simulated cardiac cycle.

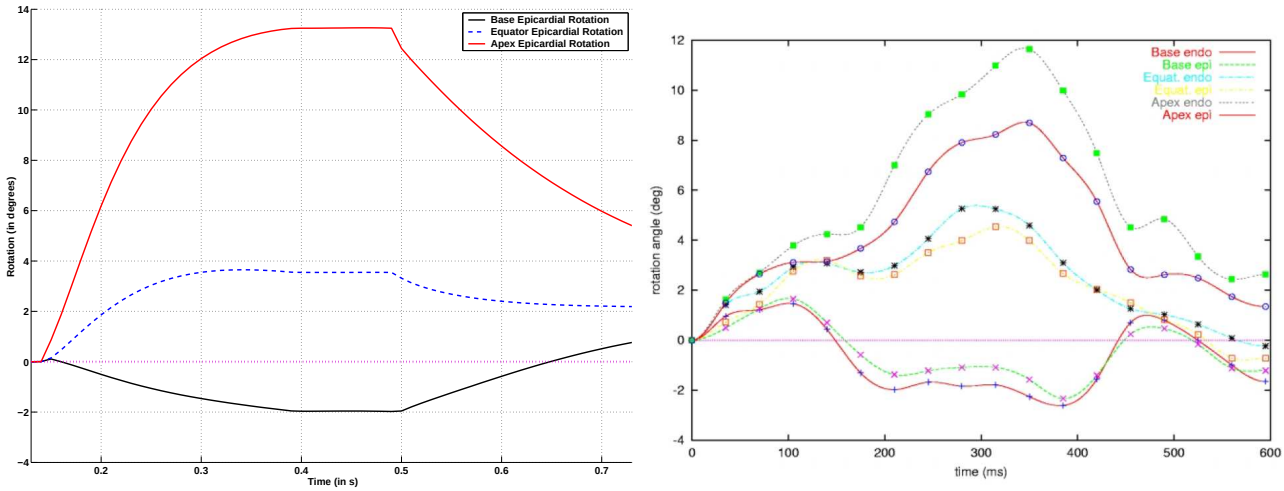

Figure 14: (Left) Twisting angle during the simulated cycle, for different points of the epicardium: base (black), equator (dashed blue) and apex (red). (Right) Twisting angle extracted from tagged MRI by Philips Research France for different points of the myocardium.

and in the measures. This twisting motion originates from the fibre orientations but also from the isovolumetric phase and the activation sequence. The simulation of the action potential propagation and the inclusion of the different phases of the cardiac cycle is thus important to recover local parameters of the cardiac motion.

5.2.3 Local Radial Contraction

Another important local parameter of the cardiac function is the radial contraction, which measures the variation of the distance from a point to the central axis, throughout the cardiac cycle. The same inertia axis as for the rotation is used to compute the radial contraction of three points of the left ventricle endocardium (Fig. 15) during the simulated cycle.

The same radial contraction was measured for different points of the myocardium by Philips Research France through the analysis of tagged MRIs [2].

The comparison of the simulated radial contraction with the measured one gives also a good correlation (Fig. 16), which confirms the fact that the simulated ejection fraction is close to the real ones and that the model has a good local behaviour. This radial contraction is responsible for the evolution of the wall thickness during the cardiac cycle, which is also a clinical index of the cardiac function.

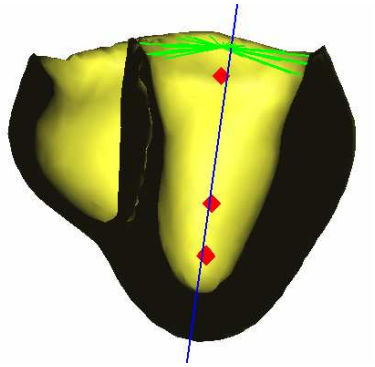

Figure 15: Basal, equatorial and apical points of the left ventricle endocardium used to observe the local radial contraction during the simulated cardiac cycle.

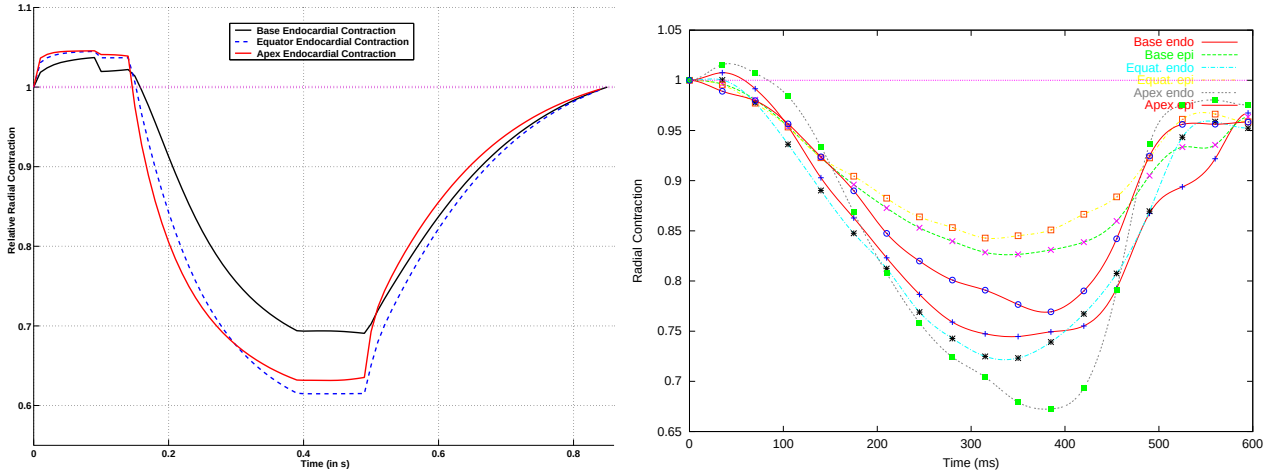

Figure 16: (Left) Radial contraction during the simulated cycle for different points of the endocardium: base (black), equator (blue - -) and apex (red). (Right) Radial contraction extracted from tagged MRI by Philips Research France for different points of the myocardium.

6 Application to Pathology Simulation and Intervention Planning

Such a model enables the simulation of different cardiovascular pathologies, at the electrophysiological level or mechanical level. The observation of the consequences of these pathologies on the simulated cardiac function could help understand the phenomena, test different therapy strategies and plan interventions.

6.1 Ectopic Focus and Bundle Branch Block

Different electrophysiological disorders can be simulated. An ectopic focus can be introduced by including an additional excitation point to the normal Purkinje extremities, with its own excitation sequence (Fig. 17 left). A bundle branch block can be simulated by removing the Purkinje network extremities in one of the ventricles, and observe the resulting depolarisation (Fig. 17 right).

6.2 Fibrillation

It has been shown that some cases of cardiac fibrillation are the result of a spiral of depolarisation meandering in the myocardium. Such spirals can be simulated with the chosen model, using appropriate initial conditions like the wave-break method (Fig. 18) [34]. Studies of these spirals could help design more efficient defibrillators [18], by using a better defibrillation timing and thus less energy.

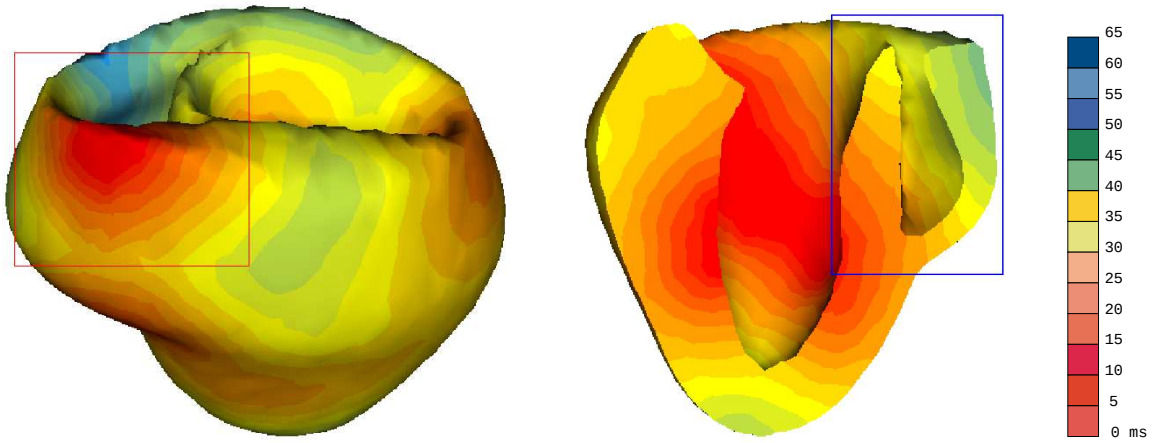

Figure 17: Electrophysiological pathologies simulation, presented with resulting isochrones. (Left) Ectopic focus (part of a Wolff-Parkinson-White syndrome simulation). (Right) Right branch block simulation.

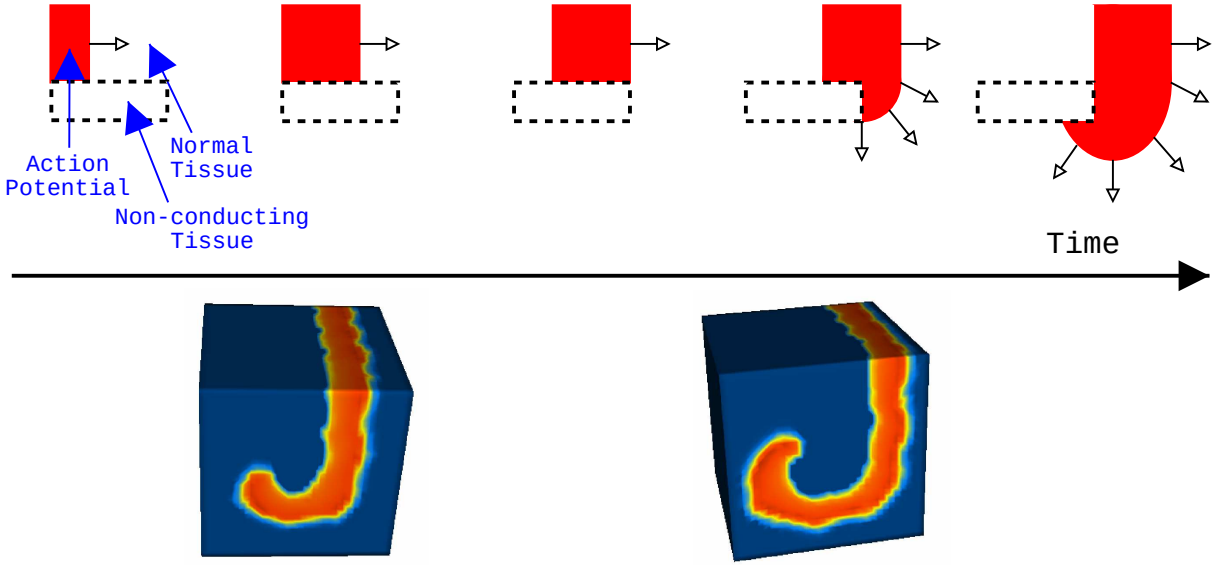

Figure 18: Simulation of a reentry spiral using a «wave-break». (Top) Description of the wave-break method. (Bottom) Simulation on a cube of myocardium model. Colour represents the action potential (light red: depolarised, dark blue: re polarised).

6.3 Radio-Frequency Ablation

Most of the ventricular electrophysiological pathologies are not easily treated, and the radio-frequency ablation procedure is often lengthy, which results in considerable X ray doses delivered and with an uncertain outcome. Simulating the pathology and the outcome of different ablation strategies could help for the planning of such interventions. The presented model was coupled with a force-feedback 3D interface (Phantom from Sensable Technologies). It allows one to point locations in 3D on the model and change in real time the conductivity of these locations, whilst the simulation is running (Fig. 19).

6.4 Infarcted Area

Some tissue pathologies, like infarcted areas, can be introduced in the potential propagation and in the mechanical contraction. These regions can be observed with late-enhancement MR, thus localised in the model geometry. Infarcted tissues have an impact on the local conductivity, as well as on the passive and active mechanical properties of the myocardium. These different effects can be investigated through simulations, for

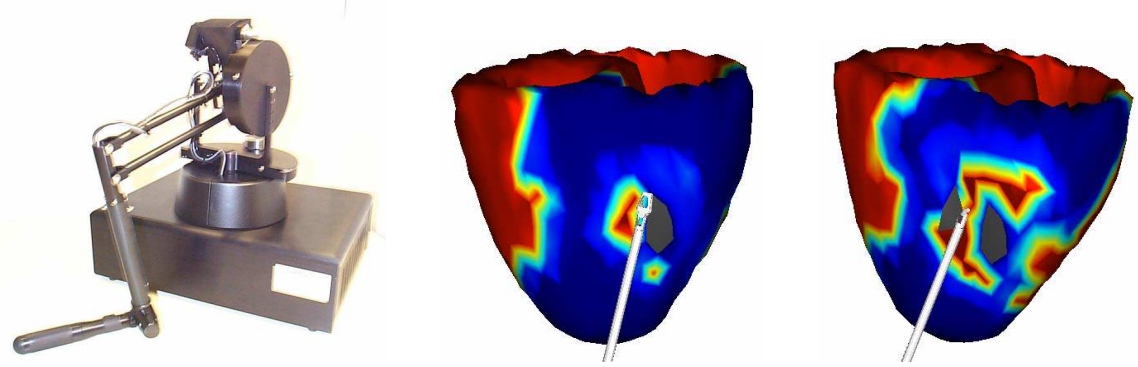

Figure 19: (Left) Phantom 3D interface, from Sensable Technologies. (Right) Radio-frequency ablation simulation, by modifying the conducting parameters of the model where it has been in contact with the tool (homogeneous grey areas).

example the influence on the ejection fraction, which decreases from 65% to 55% in the simulated case (Fig. 20).

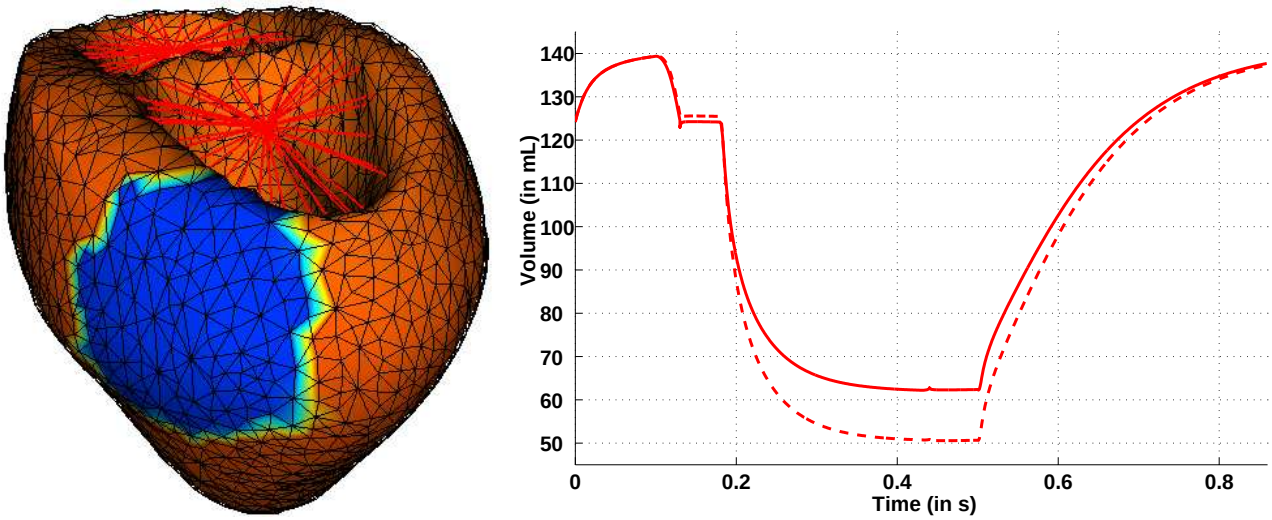

Figure 20: Basal left epicardial infarcted zone (blue) simulation. No conduction and no contraction in this area. (Right) Corresponding volume curves without (dashed) and with (solid) infarct. Ejection fraction decreases from 65% to 55%.

Validation of the simulation of these pathologies is in progress within the Cardiac MR Research Group, King's College London, Guy's Hospital, London[6] [67].

To achieve this aim, new methods have to be designed to be able to locally adjust the parameters of the model to the available data. Very promising results have been obtained on the parameter adjustment of a surface model of the epicardium electrophysiology [50], and current effort is directed at INRIA to identify electrical and mechanical parameters of the 3D model from clinical data.

7 Application to Image Analysis: a Pro-Active Deformable Model

One of the goals of building this model is to apply it to cardiac image segmentation. The key idea is to build a "Pro-Active Deformable Model" of the heart for image analysis, i.e. a volumetric deformable model of the heart integrating *a priori* knowledge on the motion, through the simulation of the electromechanical contraction. The internal energy regularising the deformation is computed from the electromechanical model previously presented

[6] http://www-ipg.umds.ac.uk/m.sermesant/index.php

and the external energy is computed from the image features. We thus solve the new dynamics equation, where these energies write as forces:

$$M\frac{d^2U}{dt^2} + C\frac{dU}{dt} + KU = F_c + \alpha F_i \tag{5}$$

with F_c the contraction forces, F_i the image forces, and α the weighting parameter for the image forces.

7.1 Internal Forces

The internal forces are computed from the electromechanical rheological model, thus introducing the simulated contraction. We use the model presented section 3.1 to compute the action potential propagation and the model of section 4.2 to compute the mechanical contraction. For the time synchronisation, information on the image sequence acquisition allows us to know the heart beat duration, the R wave position and the timing of each image in the cycle. This is used to trigger the action potential propagation and adjust the action potential duration, as well as to compute the external forces.

For this segmentation goal, some boundary conditions, like pressure and isovolumetric phases, are partly included in the image information. The added stiffness to represent the valves is also a part of the image information. This is the reason why no mechanical boundary conditions other than image forces are applied when the model is used in this image analysis framework.

Usually, segmentation methods use one rest position of the model per image, corresponding to the previous image final position. We believe it is important not to reset the strain and stress at each time frame in order to capture all the characteristics of the deformation of the myocardium. Thus we want to use only one rest position of the heart for the complete sequence.

Due to the large difference in shape between the tele-diastolic position and the tele-systolic position, using *a priori* knowledge on the motion helps recover this deformation, as the image forces only have to correct the predicted deformation, not create it from the tele-diastolic shape.

7.2 External Forces

The external forces are introduced as a load applied to the mechanical model. For each surface node of the mesh, we look for a corresponding boundary point in the image voxels lying along the surface normal, a classical approach for deformable models in computer vision. The boundary point is selected among these voxels from intensity, gradient direction and gradient value criteria [49]. Then a force is applied to this node, proportional to the distance to this boundary voxel and oriented in its direction.

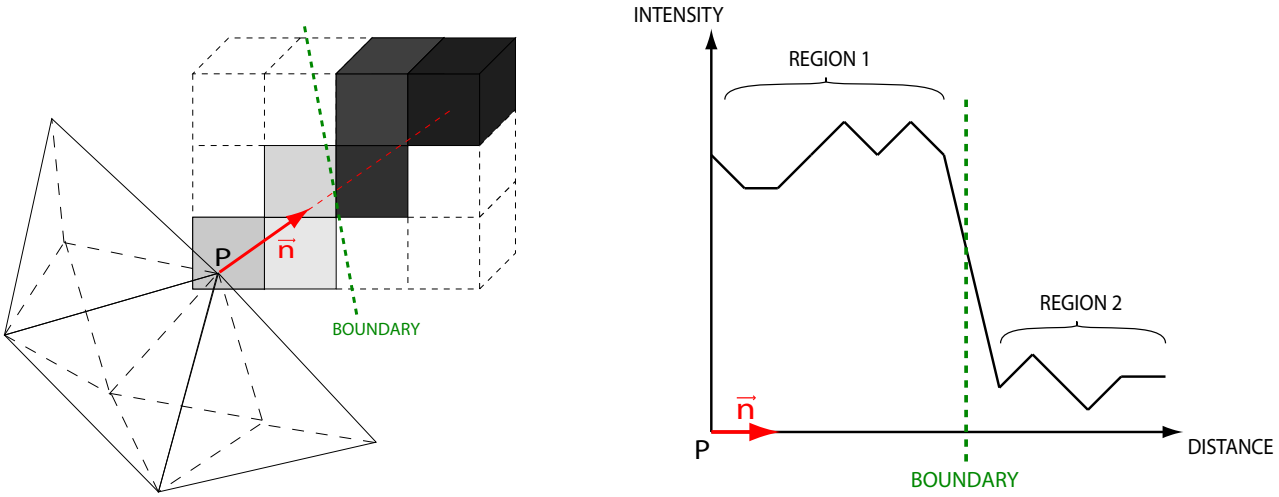

Figure 21: External forces computation. (Left) Scan-line algorithm to extract the image voxels from a vertex P along the normal $\vec{n}$ to the mesh surface. (Right) Region and boundary criteria on the extracted voxels to determine the boundary point corresponding to the surface vertex P.

These forces can be different on each of the different anatomical regions of the model, depending on what is visible in the different parts of the image and on the image intensity characteristics in these regions. If some

parts of the myocardium are not visible, the external forces can be removed for the corresponding regions and only the internal forces will make these vertices evolve.

7.3 Global Adjustment to Patient Anatomy

The correspondences between the surface nodes and the boundary voxels can be used to globally adjust the mesh to the patient anatomy. After a rough alignment of the ventricles, we compute iteratively the best rigid transformation between the mesh and the image. After convergence, we compute the best similarity and finally the best affine transform. We use a new criterion proposed by X. Pennec and presented in [66].

7.4 Sequence Segmentation: Time-continuous Image Force Field

As we use an electromechanical model for the internal energy, we need to integrate it according to time steps given by stability constraints, which are independent from the image acquisition time resolution. We create a "time-continuous image force field" by using the two images of the sequence surrounding the current integrated time in the cycle to interpolate the force to apply from the two forces computed within each of these images. This ensures a smooth evolution of the mechanical boundary conditions, thus a better stability and segmentation process.

If we have an image I_1 at instant t_1 and the next one I_2 is at instant t_2, and the segmentation process is at time t in the cardiac cycle, between t_1 and t_2, then the applied image force is:

$$F_i(t) = \frac{1}{t_2 - t_1}\left[(t_2 - t)F_{I_1}(t) + (t - t_1)F_{I_2}(t)\right]$$

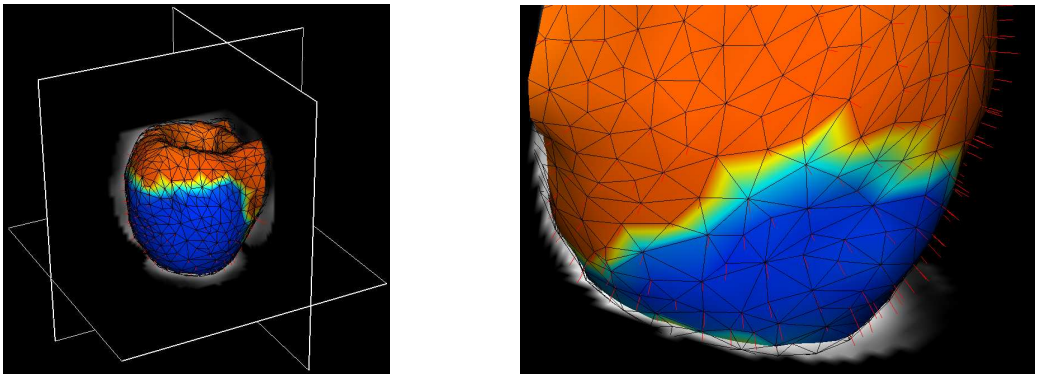

Figure 22: Segmentation of cardiac image sequence with the pro-active model of the heart. The model is displayed with slices of one image of the sequence, but the external forces are computed with two images. The action potential value is colour-coded on the model surface and the red segments represent the external forces on the surface vertices toward the corresponding images voxels.

7.5 Results

We present here the left ventricle volume curves obtained when segmenting a SPECT image sequence with a passive biomechanical deformable model and with the pro-active deformable model. They are compared to "ground truth" values obtained with another segmentation method and to the electromechanical model alone. To present this proof of concept, we use SPECT imaging where boundary definition is quite clear to demonstrate the effect of the active internal forces, without to much influence of the choice of external forces.

The consequence of the introduction of *a priori* knowledge on the motion in the segmentation is a better estimation of the volume, especially of the tele-systolic position (see Fig. 23 and Fig. 24). The ejection fraction, which is an important clinical index of the cardiac function, is then more accurately computed. The ejection fraction computed from the "ground truth" is 66%. We obtain an ejection fraction of 68% with the pro-active model (the electromechanical model alone has an ejection fraction of 62%) whereas the passive model results in only 53% .

Furthermore, the needed weight of the image forces, α in equation (5), is ten times smaller with the pro-active model, because it only has to correct the predicted motion, not to create the whole deformation from the tele-diastolic position.

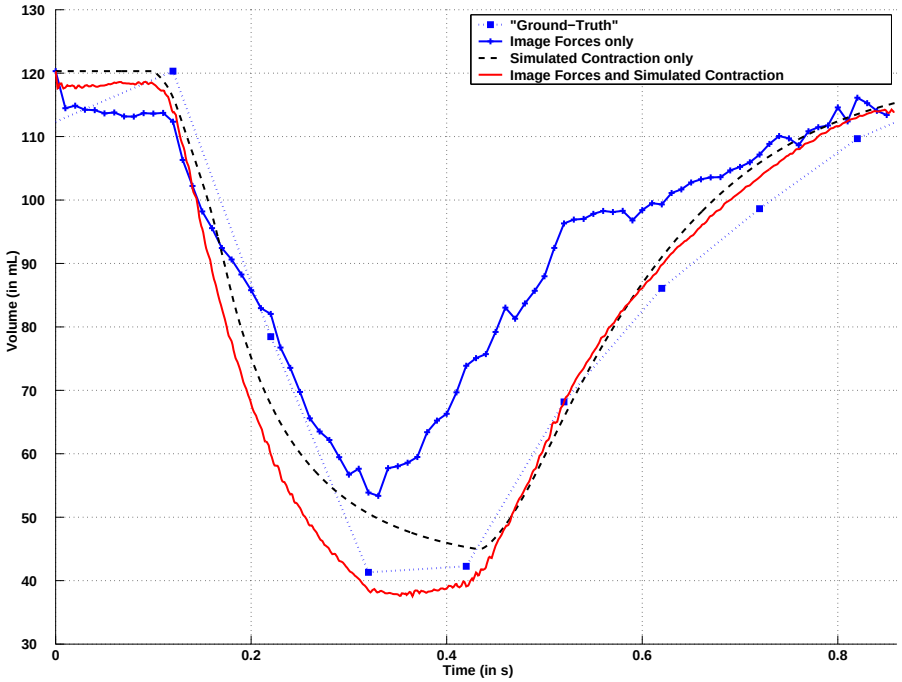

Figure 23: Comparison between the segmentation using the passive biomechanical model (blue line) and the pro-active model (red line). The "ground truth" segmentation is the blue squares, and the black dashed line shows the electromechanical model alone. The combined use of electromechanical model with image information allows a better segmentation of the image sequence.

The model evolution gives a continuous estimation of the myocardium position throughout the cardiac cycle. It allows to interpolates image information to correspond best at each time when an image is available and to continuously deform in between.

Moreover, using this pro-active model gives *a priori* information on the local tangential motion (torsion) which is hardly visible in current medical images (without using tags). This kind of model could help recover this motion, which is also quite important in cardiac function.

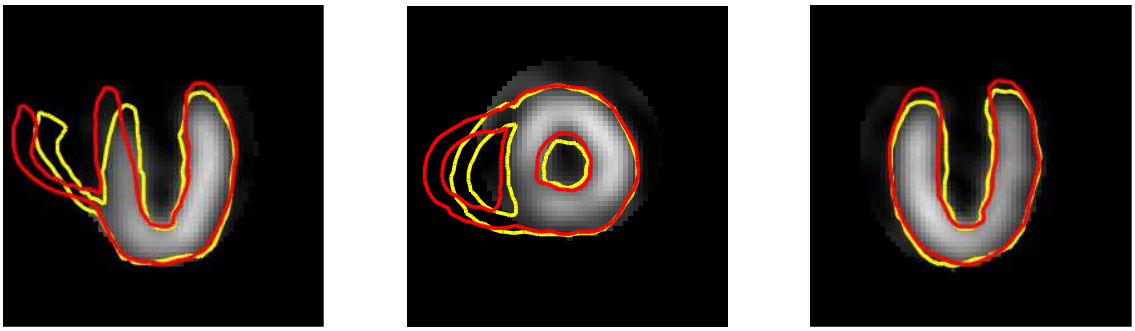

Figure 24: Comparison of the segmentation of a SPECT image sequence, in three orthogonal slices of the tele-systolic position (red: passive biomechanical model, yellow: pro-active model). The electromechanical model stays closer to the image boundary, especially near the base (axial contraction) and we can observe the right ventricle contraction of the model, even if the right ventricle is not visible in the image (due to a previous region of interest extraction).

The segmentation of a full image sequence with the pro-active model takes less than 5 minutes on a standard PC. We use a coarser mesh (10 000 elements) which is better adapted to the limited image resolution.

The isovolumetric phases are not simulated in this case, saving a significant computational cost. The whole segmentation time does not depend on the time resolution of the image sequence as only the electromechanical phenomena control the integration time steps, and then image forces are computed for each of these integrated time steps.

8 Conclusions

The design of computational models of human organs is a new research field which opens new possibilities for medical image analysis and therapy simulation: this report presented a number of steps toward this goal in cardiac imagery, and must be understood as a preliminary proof of concept in this research direction.

The model we presented was designed at a macroscopic level with a limited number of internal parameters which still allowed a realistic direct simulation of the heart motion while allowing reasonable computing time. We also showed that our "pro-active" deformable model using its internal contraction forces synchronised on the ECG was able to better recover the segmentation of the heart ventricles from a time series of cardiac images than a more classical "passive" deformable model which would deform under the action of image forces only.

Finally, our model was designed to allow the future study of the automatic identification of its internal parameters from a number of clinical measurements, in order to create patient-specific heart models. Current work in this direction is already very promising [50, 61, 68].

Acknowledgements

The authors would like to thank for their collaboration Dr. Edward Hsu from Duke University; Pr. Andrew McCulloch from University of California, San Diego; Pr. Karl-Heinz Höhne and his group from Hamburg University; Dr. Olivier Gérard and Philips Medical Systems Research Paris; the Cardiac MR Research Group in Guy's Hospital, London and all the co-workers of the ICEMA collaborative research actions[7,8] funded by INRIA, in particular F. Clément, M. Sorine, Y. Coudière, D. Chapelle, J. Sainte-Marie, R. Cimrman, S. Lantéri, and Z. Li. The authors would like to thank Timothy Carter, Olivier Clatz and Philippe Moireau for thoughtful comments, and Rado Andriantsimiavona for left ventricle volume segmentation from cardiac MRI.

Colour version of the presented figures and video animations are available on the internet[9].

References

[1] R. Aliev and A. Panfilov. A simple two-variable model of cardiac excitation. *Chaos, Solitons & Fractals*, 7(3):293–301, 1996.

[2] C. Allouche, S. Makram, N. Ayache, and H. Delingette. A new kinetic modeling scheme for the human left ventricle wall motion with MR-tagging imaging. In *Functional Imaging and Modeling of the Heart (FIMH'01)*, number 2230 in Lecture Notes in Computer Science (LNCS), pages 61–68. Springer, 2001.

[3] R. Andriantsimiavona, L. Griffin, D. Hill, and R. Razavi. Simple cardiac MRI segmentation. In *International Society for Magnetic Resonance in Medicine Scientific Meeting*, volume 6, page 951, 2003.

[4] N. Ayache, editor. *Computational Models for the Human Body.* Handbook of Numerical Analysis (P. Ciarlet series editor). Elsevier, 2004.

[5] F. Azar, D. Metaxas, and M. Schnall. Methods for modeling and predicting mechanical deformations of the breast under external perturbations. *Medical Image Analysis*, 6(1):1–27, 2002.

[6] G. W. Beeler and H. Reuter. Reconstruction of the action potential of ventricular myocardial fibers. *Journal of Physiology*, 268:177–210, 1977.

[7] J. Bestel, F. Clément, and M. Sorine. A biomechanical model of muscle contraction. In *Medical Image Computing and Computer-Assisted intervention (MICCAI'01)*, volume 2208 of *Lecture Notes in Computer Science (LNCS)*, pages 1159–1161. Springer, 2001.

[7] http://www-rocq.inria.fr/who/Frederique.Clement/icema.html
[8] http://www-rocq.inria.fr/sosso/icema2/icema2.html
[9] http://www-sop.inria.fr/epidaure/personnel/Maxime.Sermesant/gallery.php

[8] D. Caillerie, A. Mourad, and A. Raoult. Towards a fibre-based constitutive law for the myocardium. In *Modelling & Simulation for Computer-aided Medicine and Surgery (MS4CMS'02)*, volume 12, pages 25–30. ESAIM Proceedings, 2002.

[9] D. Chapelle, F. Clément, F. Génot, P. Le Tallec, M. Sorine, and J. Urquiza. A physiologically-based model for the active cardiac muscle contraction. In *Functional Imaging and Modeling of the Heart (FIMH'01)*, number 2230 in Lecture Notes in Computer Science (LNCS), pages 128–133. Springer, 2001.

[10] T. Cootes and C. Taylor. Statistical models of appearance for medical image analysis and computer vision. In M. Sonka and K. Hanson, editors, *Proceedings of SPIE Medical Imaging*, volume 4322, pages 236–248, 2001.

[11] D. Durrer, R. van Dam, G. Freud, M. Janse, F. Meijler, and R. Arzbaecher. Total excitation of the isolated human heart. *Circulation*, 41(6):899–912, 1970.

[12] O. Faris, F. Evans, D. Ennis, P. Helm, J. Taylor, A. Chesnick, M. Guttman, C. Ozturk, and E. McVeigh. Novel technique for cardiac electromechanical mapping with magnetic resonance imaging tagging and an epicardial electrode sock. *Annals of Biomedical Engineering*, 31(4):430–440, 2003.

[13] M. Ferrant, A. Nabavi, B. Macq, F. Jolesz, R. Kikinis, and S. Warfield. Registration of 3D intraoperative MR images of the brain using a finite element biomechanical model. *IEEE Transactions on Medical Imaging*, 20:1384–1397, 2001.

[14] R. FitzHugh. Impulses and physiological states in theoretical models of nerve membrane. *Biophysical Journal*, 1:445–466, 1961.

[15] A. Frangi, W. Niessen, and M. Viergever. Three-dimensional modeling for functional analysis of cardiac images: A review. *IEEE Transactions on Medical Imaging*, 1(20):2–25, 2001.

[16] A. Frangi, D. Rueckert, and J. Duncan, editors. *New Trends in Three-Dimensional Cardiac Image Analysis*, volume 21(9). IEEE Transactions on Medical Imaging, 2003.

[17] O. Gérard, A. Collet Billon, J.-M. Rouet, M. Jacob, M. Fradkin, and C. Allouche. Efficient model-based quantification of left ventricle function in 3D echography. *IEEE Transactions on Medical Imaging*, 21(9):1059–1068, 2002.

[18] G. Gottwald, A. Pumir, and V. Krinsky. Spiral wave drift induced by stimulating wave trains. *Chaos*, 11(3):487–494, 2001.

[19] J. Guccione and A. McCulloch. *Theory of Heart: biomechanics, biophysics, and nonlinear dynamics of cardiac function*, chapter Finite element modeling of ventricular mechanics, pages 121–144. Springer-Verlag, 1991.

[20] J. Häfner, F. Sachse, C. Sansour, G. Seemann, and O. Dössel. Hyperelastic description of elastomechanic properties of the heart: A new material law and its application. *Biomedizinische Technik*, 47-1/2:770–773, 2002.

[21] G. Hamarneh and T. Gustavsson. Deformable spatio-temporal shape models: Extending ASM to 2D+time. *Journal of Image and Vision Computing*, 22(6):461–470, 2004.

[22] A. Hodgkin and A. Huxley. A quantitative description of membrane current and its application to conduction and excitation in nerve. *Journal of Physiology*, 177:500–544, 1952.

[23] E. Hsu and C. Henriquez. Myocardial fiber orientation mapping using reduced encoding diffusion tensor imaging. *Journal of Cardiovascular Magnetic Resonance*, 3:325–333, 2001.

[24] J. Humphrey, R. Strumpf, and F. Yin. Determination of a constitutive relation for passive myocardium: I. A new functional form. *ASME Journal of Biomechanical Engineering*, 112:333–339, 1990.

[25] P. Hunter, M. Nash, and G. Sands. *Computational Biology of the Heart*, chapter 12: Computational Electromechanics of the Heart, pages 345–407. John Wiley & Sons, 1997.

[26] P. Hunter, A. Pullan, and B. Smaill. Modeling total heart function. *Annual Review of Biomedical Engineering*, 5:147–177, 2003.

[27] P. Hunter and B. Smaill. The analysis of cardiac function: a continuum approach. *Progress in Biophysics and Molecular Biology*, 52:101–164, 1988.

[28] G. Jacob, J.A. Noble, C. Behrenbruch, A. Kelion, and A. Banning. A shape-space-based approach to tracking mycordial borders and quantifying regional left-ventricular function applied in echocardiography. *IEEE Transactions on Medical Imaging*, 21(3):226–238, 2002.

[29] M.-P. Jolly, N. Duta, and G. Funka-Lea. Segmentation of the left ventricle in cardiac MR images. In *Proceedings of the IEEE International Conference on Computer Vision (ICCV'01)*, 2001.

[30] T. Katila, I. Magnin, P. Clarysse, J. Montagnat, and J. Nenonen, editors. *Functional Imaging and Modeling of the Heart (FIMH'01)*, number 2230 in Lecture Notes in Computer Science (LNCS). Springer, 2001.

[31] M. Kaus, J. von Berg, J. Weese, W. Niessen, and V. Pekar. Automated segmentation of the left ventricle in cardiac MRI. *Medical Image Analysis*, 8(3):245–254, 2004.

[32] P. Kilner, G.Z. Yang, A. Wilkes, R. Mohiaddin, D. Firmin, and M. Yacoub. Asymmetric redirection of flow through the heart. *Nature*, 404:759–761, 2000.

[33] Z. Knudsen, A. Holden, and J. Brindley. Qualitative modelling of mechano-electrical feedback in a ventricular cell. *Bulletin of Mathematical Biology*, 6(59):115–181, 1997.

[34] V. Krinsky. Spread of excitation in an inhomogeneous medium (state similar to cardiac fibrillation). *Biofizika*, 11:676–683, 1966.

[35] B. Lelieveldt, S. Mitchell, J. Bosch, R. van der Geest, M. Sonka, and J. Reiber. Time continuous segmentation of cardiac image sequences using active appearance motion models. In *Proceedings of Information Processing in Medical Imaging (IPMI'01)*, volume 2082 of *Lecture Notes in Computer Science (LNCS)*, pages 446–452. Springer, 2001.

[36] H. Liu and P. Shi. Meshfree representation and computation: Applications to cardiac motion analysis. In *Information Processing in Medical Imaging (IPMI'03)*, volume 2732 of *Lecture Notes in Computer Science (LNCS)*. Springer, 2003.

[37] H. Liu and P. Shi. Simultaneous estimation of left ventricular motion and material properties with maximum a posteriori strategy. In *IEEE Computer Vision and Pattern Recognition*, 2003.

[38] E. Lo, H. Liu, and P. Shi. H∞ filtering and physical modeling for robust kinematics estimation. In *IEEE International Conference on Image Processing*, 2003.

[39] W. Lorensen and H. Cline. Marching cubes: a high resolution 3D surface reconstruction algorithm. *Computer Graphics (Proc. of SIGGRAPH)*, 21(4):163–169, 1987.

[40] C. Luo and Y. Rudy. A model of the ventricular cardiac action potential: depolarization, repolarization, and their interaction. *Circulation Research*, 68:1501–1526, 1991.

[41] R. MacLeod, B. Yilmaz, B. Taccardi, B. Punske, Y. Serinagaolu, and D. Brooks. Direct and inverse methods for cardiac mapping using multielectrode catheter measurements. *Journal of Biomedizinische Technik*, 46:207–209, 2001.

[42] I. Magnin, J. Montagnat, P. Clarysse, J. Nenonen, and T. Katila, editors. *Functional Imaging and Modeling of the Heart (FIMH'03)*, number 2674 in Lecture Notes in Computer Science (LNCS). Springer, 2003.

[43] S. Masood, G.Z. Yang, D. Pennell, and D. Firmin. Investigating intrinsic myocardial mechanics: the role of MR tagging, velocity phase mapping and diffusion imaging. *Journal of Magnetic Resonance Imaging*, 12(6):873–883, 2000.

[44] A. McCulloch, J.B. Bassingthwaighte, P.J. Hunter, D. Noble, T.L. Blundell, and T. Pawson. Computational biology of the heart: From structure to function. *Progress in Biophysics & Molecular Biology*, 69(2/3):151–559, 1998.

[45] T. McInerney and D. Terzopoulos. Deformable models in medical images analysis: a survey. *Medical Image Analysis*, 1(2):91–108, 1996.

[46] M. Mignotte, J. Meunier, and J.-C. Tardif. Endocardial boundary estimation and tracking in echocardiographic images using deformable templates and markov random fields. *Pattern Analysis and Applications*, 4(4):256–271, 2001.

[47] J. Montagnat and H. Delingette. Space and time shape constrained deformable surfaces for 4D medical image segmentation. In *Medical Image Computing and Computer-Assisted Intervention (MICCAI'00)*, volume 1935 of *Lecture Notes in Computer Science (LNCS)*, pages 196–205. Springer, 2000.

[48] J. Montagnat and H. Delingette. A review of deformable surfaces: topology, geometry and deformation. *Image and Vision Computing*, 19(14):1023–1040, 2001.

[49] J. Montagnat, M. Sermesant, H. Delingette, G. Malandain, and N. Ayache. Anisotropic filtering for model-based segmentation of 4D cylindrical echocardiographic images. *Pattern Recognition Letters*, 24:815–828, 2003.

[50] V. Moreau-Villéger, H. Delingette, M. Sermesant, O. Faris, E. McVeigh, and N. Ayache. Global and local parameter estimation of a model of the electrical activity of the heart. Technical report, INRIA, 2004.

[51] M. Nash. *Mechanics and Material Properties of the Heart using an Anatomically Accurate Mathematical Model.* PhD thesis, University of Auckland, 1998.

[52] P. Nielsen, I. Le Grice, B. Smail, and P. Hunter. Mathematical model of geometry and fibrous structure of the heart. *American Journal of Physiology*, 260(29):1365–1378, 1991.

[53] D. Noble. Modeling the heart. *Physiology*, 19:191–197, 2004.

[54] D. Noble, A. Varghese, P. Kohl, and P. Noble. Improved guinea-pig ventricular cell model incorporating a diadic space, I_{Kr} and I_{Ks}, and length and tension dependent processes. *Canadian Journal of Cardiology*, 14:123–134, 1998.

[55] X. Papademetris, A. J. Sinusas, D. P. Dione, and J. S. Duncan. Estimation of 3D left ventricle deformation from echocardiography. *Medical Image Analysis*, 5(1):17–28, 2001.

[56] J. Park, D. Metaxas, and L. Axel. Analysis of left ventricular wall motion based on volumetric deformable models and MRI-SPAMM. *Medical Image Analysis*, pages 53–71, 1996.

[57] K. Park, D. Metaxas, and L. Axel. A finite element model for functional analysis of 4D cardiac-tagged MR images. In *Medical Image Computing and Computer-Assisted Intervention (MICCAI'03)*, volume 2878 of *Lecture Notes in Computer Science (LNCS)*, pages 491–498. Springer, 2003.

[58] Q.C. Pham, F. Vincent, P. Clarysse, P. Croisille, and I. Magnin. A FEM-based deformable model for the 3D segmentation and tracking of the heart in cardiac MRI. In *Image and Signal Processing and Analysis (ISPA'01)*, 2001.

[59] A. Pommert, K.-H. Höhne, B. Pflesser, E. Richter, M. Riemer, T. Schiemann, R. Schubert, U. Schumacher, and U. Tiede. Creating a high-resolution spatial/symbolic model of the inner organs based on the visible human. *Medical Image Analysis*, 5(3):221–228, 2001.

[60] K. Rhode, D. Hill, P. Edwards, J. Hipwell, D. Rueckert, G. Sanchez-Ortiz, S. Hegde, V. Rahunathan, and R. Razavi. Registration and tracking to integrate X-ray and MR images in an XMR facility. *IEEE Transactions on Medical Imaging*, 22(11):1369–78, 2003.

[61] K. Rhode, M. Sermesant, G. Sanchez-Ortiz, S. Hegde, D. Rueckert, D. Hill, and R. Razavi. XMR guided cardiac electrophysiology study and radio frequency ablation. In A. Amini, editor, *SPIE Medical Imaging*, 2004.

[62] K. Sagawa, R. Lie, and J. Schaefer. Translation of Otto Frank's paper "Die grundform des arteriellen pulses" Zeitschrift fur Biologie 37:483-526 (1899). *Journal of Molecular and Cellular Cardiology*, 22(3):253–277, 1990.

[63] G. Sanchez-Ortiz, G. Wright, N. Clarke, J. Declerck, A. Banning, and J.A. Noble. Automated 3D echocardiography analysis compared with manual delineations and SPECT MUGA. *IEEE Transactions on Medical Imaging*, 21(9):1069–1076, 2002.

[64] M. Sermesant, Y. Coudière, H. Delingette, N. Ayache, J. Sainte-Marie, D. Chapelle, F. Clément, and M. Sorine. Progress towards model-based estimation of the cardiac electromechanical activity from ECG signals and 4D images. In *Modelling & Simulation for Computer-aided Medicine and Surgery (MS4CMS'02)*, volume 12, pages 153–161. ESAIM Proceedings, 2002.

[65] M. Sermesant, O. Faris, F. Evans, E. McVeigh, Y. Coudière, H. Delingette, and N. Ayache. Preliminary validation using *in vivo* measures of a macroscopic electrical model of the heart. In *International Symposium on Surgery Simulation and Soft Tissue Modeling (IS4TM'03)*, number 2230 in Lecture Notes in Computer Science (LNCS). Springer, 2003.

[66] M. Sermesant, C. Forest, X. Pennec, H. Delingette, and N. Ayache. Deformable biomechanical models: Application to 4D cardiac image analysis. *Medical Image Analysis*, 7(4):475–488, 2003.

[67] M. Sermesant, K. Rhode, A. Anjorin, S. Hegde, G. Sanchez-Ortiz, D. Rueckert, P. Lambiase, C. Bucknall, D. Hill, and R. Razavi. Simulation of the electromechanical activity of the heart using XMR interventional imaging. In *Medical Image Computing and Computer-Assisted Intervention (MICCAI'04)*, Lecture Notes in Computer Science (LNCS). Springer, 2004. to appear.

[68] M. Sermesant, K. Rhode, S. Hegde, G. Sanchez-Ortiz, D. Rueckert, P. Lambiase, C. Bucknall, D. Hill, and R. Razavi. Modelling the cardiac electromechanical activity for integration of electrophysiological studies with MR. In *International Society for Magnetic Resonance in Medicine Scientific Meeting*, volume 7, page 1890, 2004.

[69] S. Silbernagl and A. Despopoulos. *Color Atlas of Physiology.* Thieme Medical Publisher, 1991.

[70] A. Sitek, G. Klein, G. Gullberg, and R. Huesman. Deformable model of the heart with fiber structure. *IEEE Transactions on Nuclear Science*, 49(3), 2002.

[71] O. Skrinjar, A. Nabavi, and J. Duncan. Model-driven brain shift compensation. *Medical Image Analysis*, 6(4):361–373, 2002.

[72] N. Stergiopulos, B. Westerhof, and N. Westerhof. Total arterial inertance as the fourth element of the windkessel model. *American Journal of Physiology*, 276:H81–8, 1999.

[73] O. Zienkiewicz and R. Taylor. *The Finite Element Method.* McGraw-Hill, London, UK, fourth edition, 1994.

Unité de recherche INRIA Sophia Antipolis
2004, route des Lucioles - BP 93 - 06902 Sophia Antipolis Cedex (France)

Unité de recherche INRIA Futurs : Parc Club Orsay Université - ZAC des Vignes
4, rue Jacques Monod - 91893 ORSAY Cedex (France)
Unité de recherche INRIA Lorraine : LORIA, Technopôle de Nancy-Brabois - Campus scientifique
615, rue du Jardin Botanique - BP 101 - 54602 Villers-lès-Nancy Cedex (France)
Unité de recherche INRIA Rennes : IRISA, Campus universitaire de Beaulieu - 35042 Rennes Cedex (France)
Unité de recherche INRIA Rhône-Alpes : 655, avenue de l'Europe - 38334 Montbonnot Saint-Ismier (France)
Unité de recherche INRIA Rocquencourt : Domaine de Voluceau - Rocquencourt - BP 105 - 78153 Le Chesnay Cedex (France)

Éditeur
INRIA - Domaine de Voluceau - Rocquencourt, BP 105 - 78153 Le Chesnay Cedex (France)
http://www.inria.fr
ISSN 0249-6399